

# Application of a Stereo PIV System for Investigations of Flow Fields in Towing Tank and Cavitation Tunnel

P. ANSCHAU<sup>A</sup> AND K.-P. MACH<sup>A</sup>

<sup>A</sup>Potsdam Model Basin, Marquardtter Chaussee 100, 14469 Potsdam  
[anschau@sva-potsdam.de](mailto:anschau@sva-potsdam.de), [mach@sva-potsdam.de](mailto:mach@sva-potsdam.de)

A newly installed submersible stereo PIV system, designed for the use in the towing tank and operating perpendicular to the main flow direction, is described. This Stereo Particle Image Velocimetry system allows the contactfree, 3-dimensional determination of velocity fields in the towing tank and cavitation tunnel. Flow conditions can be analyzed with a resolution of a few thousand points simultaneously, with a frame rate of up to 15 pictures per second, providing a good insight into flow characteristics without disturbing the flow. The paper will describe two applications of the system that have already been carried out (propeller in open water condition and in the cavitation tunnel) and will discuss merits and disadvantages of the new system. The potentials for validation of CFD calculations will be shortly discussed. Future plans for further applications of the system will be introduced.

Keywords: Particle Image Velocimetry, Stereoscopic PIV, Fluid Mechanics, Ship Hydrodynamics

## 1. Introduction

Thorough knowledge of flow conditions is an important prerequisite for competitive ship and propeller design. Measurements of velocity fields behind a model ship with and without working propeller are usually done with a conventional five-hole pressure probe. It is easy and quickly to use but gives only time averaged results with comparably poor spatial resolution; moreover it disturbs the flow field and cannot give the necessary insight into flow separation phenomena. Additionally, inflow directions of only up to 25° can be measured. A more advanced technique is the "Laser Doppler Velocimetry" (LDV), which has been successfully applied at the Potsdam Model Basin for many years [1]. While the resolution in time and space can be very high when using LDV (which can be useful for the investigation of unsteady periodic flow phenomena), determination of velocity fields in a larger area and/or with high spatial resolution becomes very time-consuming. The investigation of a greater variety of conditions (different operating points, rudder and drift angles, in various combinations) is virtually not practicable respectively affordable in this way. Conventional *two*-dimensional PIV measurements are not satisfying for the mentioned purposes because perspective errors cannot be corrected from the measured velocity field and the third velocity component is not obtainable at all.

To overcome these limitations a new Stereo Particle Image Velocimetry (SPIV) system from TSI was installed at Potsdam Model Basin which allows the contactfree,

3-dimensional determination of velocity fields in both the towing tank and the cavitation tunnel. The system allows the exploration of flow conditions with a resolution of several thousand points simultaneously. The size of the physical area being watched depends on the kind of optics being used. The double frame rate is up to 15 pictures per second, which is not sufficient for high frequency transient phenomena, but provides a good insight into flow characteristics without disturbing the flow. This way time averaged flow fields can be measured with a considerable spatial resolution. Thanks to its modular design, the system can be set up in several ways, thus allowing for symmetric as well as asymmetric configuration of cameras and lightsheet (see Fig. 1).

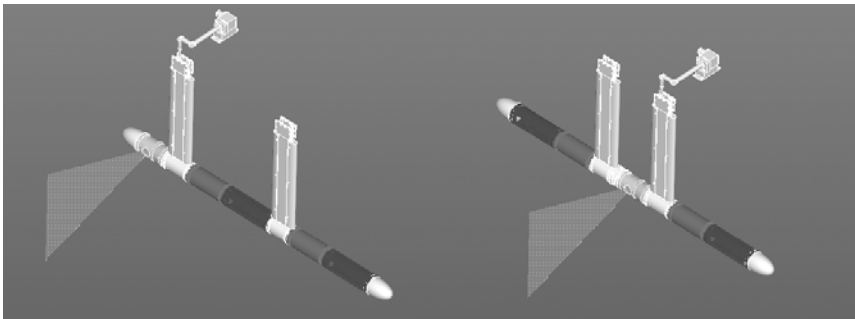


Fig. 1 Two out of several possible arrangements of the modular SPIV system [2].  
*Left:* Cameras on same side of lightsheet. *Right:* Symmetric, cameras on both sides.

In this paper we will describe two experimental setups for which SPIV measurements were conducted: a) Open water tests in the towing tank and b) the cavitation tunnel. Roughly similar experiments in a circulating water channel have been reported already in [3], but were conducted in a very different flow regime. In our experiments all four „quadrants” (positive/negative direction of inflow and rotation) of operating conditions of the propeller were investigated. We will present selected results and additionally will compare these to CFD calculations. Finally, we will take a short look at future applications of the system.

## 2. Experimental Set-up

With PIV technique the velocity field is measured by capturing two consecutive pictures of the same illuminated area in the fluid. Illumination is done with a light sheet generated by a laser beam which is spread by a cylindrical lens. The fluid needs to be seeded with small particles that reflect the laser light. The displacement of the particle images between the two pictures is measured using cross correlation methods, and with the known  $\Delta t$  the velocity field can be calculated. If two cameras are used (i.e. stereo PIV is applied), even the out of plane displacement of the particles can be calculated.

Table 1. Main experimental conditions in open water and cavitation tunnel propeller test.

		Open water test	Cavitation tunnel	Unit
Propeller	advance coefficient	0.3	varying	—
Laser	laser type	Nd:YAG	Nd:YAG	—
	max. power	190	190	mJ/puls
	max. pulse repetition rate	15	15	Hz
Recording	focal width (cam1/cam2)	55/105	28/28	mm
	viewing angle between cams.	15	20	degree
	resolution	1200x1600	1200x1600	px <sup>2</sup>
	max. double frame capt. rate	15	15	frames/s
	converging lens focal length	1000	500/1000	mm
	cylindrical lens focal length	50	25	mm
	viewing area at light sheet	160x250	~210x330	mm <sup>2</sup>
Analysis	interrogation window size	32x32	32x32	px <sup>2</sup>
	equivalent physical area	4.8x4.8	6x6	mm <sup>2</sup>
Plane of observation	position of light sheet	0.2/0.4/0.6 D <sub>p</sub> behind	centerline	—
	plane of light sheet	YZ	XZ	—

## 2.1. Open water test

A schematic sketch of the SPIV system setup for use in the towing tank is shown in Fig. 2; an overview of experimental conditions is given in Table 1. The system consists of a submersible tube (120 mm diameter, 2300 mm length) fixed at two streamlined struts which allow an operating depth of up to 0.7 m (see Fig. 3). The tube contains the two cameras, the corresponding tilted mirrors, the converging and cylindrical lenses for laser beam focusing and spreading and the mirror for the laser beam emission at the front end of the tube. The distance between the adjustable tilt mirrors was set to ~750 mm, which is a compromise between achieving the desired field of view, a possibly large angle between the two camera respectively mirror center axes and a preferably small skewness of the front camera's (CCD 1) viewing area.

The laser beam is directed from atop via a mirror tube that goes through the front strut down to the lenses, where it is first focused and then expanded to a sheet of light. The light sheet is aligned perpendicular to the main flow direction; it is generated by a dual-laser system with two frequency-doubled (532 nm), pulsed Nd:YAG lasers with a maximum energy of 190 mJ/pulse. The beams from the two lasers are combined into a collinear beam. On the one hand, with the dual-laser system the timing of the two consecutive laser pulses can be adjusted almost arbitrarily. Another advantage is the similarity of the laser intensity of the two pulses. On the other hand the alignment of the two laser beams poses a certain difficulty. Spreading of the laser beam is done with a cylindrical lens, the focal length of which can be varied between 10 mm to 50 mm. The thickness of the light sheet is about 1 mm in the measurement area but

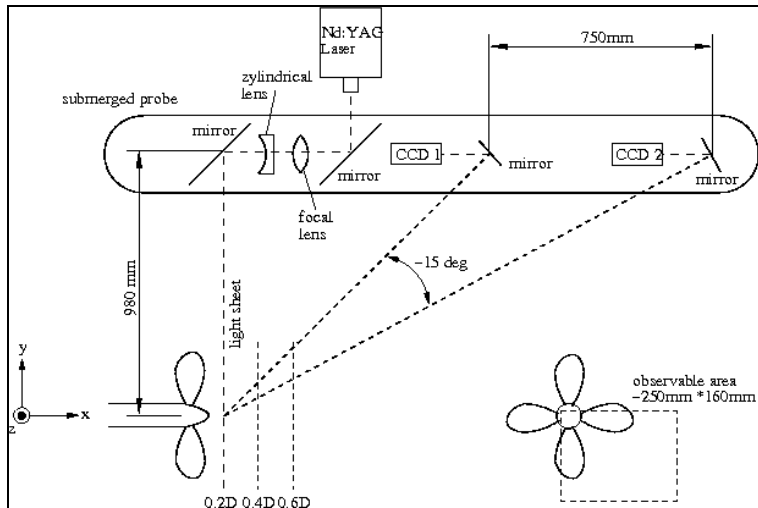


Fig. 2 Schematic sketch of experimental setup in open water test (not in scale).

varies between 0.5 mm and 2 mm, depending on the distance from the waist of the beam. Following [4], the thinner the light sheet is, the better the spatial resolution gets even in z and y direction, but the resulting signal-to-noise ratio decreases.  $\Delta t$  was adjusted after some preliminary

tests to give the highest number of measured vectors and varied between 150 and 350  $\mu s$ , depending on the investigated quadrant and the distance between light sheet and propeller plane. Also  $\Delta t$  must be selected in a way that particles will not pass the subject plane before the second capture is taken.

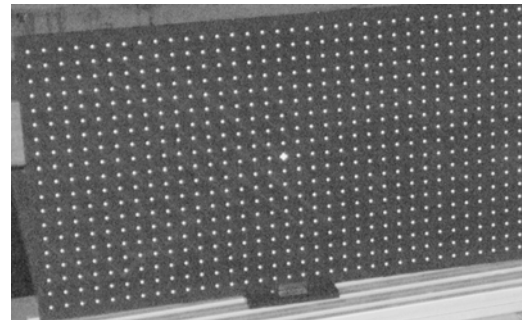


Fig. 3 SPIV probe mounted under towing carriage. Fig. 4 Calibration target, 19x34 dots, 20 mm spacing.

The two cameras being used have a resolution of 12bit/pixel and a 1200\*1600 pixel<sup>2</sup> CCD chip. The lenses are of Nikkor type. The focal length can be varied stepwise between 28 mm and 105 mm and was set to 55 mm (CCD 1) respectively 105 mm (CCD 2).

Seeding particles of about 90  $\mu m$  were used to give the necessary number of at least 10 particle images per interrogation window (the small piece of the picture being analysed with cross correlation).

The Calibration of the system is accomplished with a four plane calibration target (see Fig. 4) with a 20 mm spaced lattice of white dots aligned with diagonal bands of

alternating levels (1 mm difference) on either side. The retrieved mapping functions allow the reconstruction of the 3D vector field from the two particle displacement fields of the two cameras.

## 2.2. Cavitation tunnel

The laser and the cameras from the submersible SPIV probe were used to carry out 3D measurements in the cavitation tunnel with the same propeller as before. Fig. 5 schematically shows the arrangement of cameras and light sheet; the main difference to the previous experiment is the light sheet alignment with the propeller axis. The mirror tube of the previous experiment was not used, as the laser sheet enters through a window from below the cavitation tunnel. In this experiment, all four quadrants were investigated in front of and behind the propeller plane, providing a more detailed insight also into the propeller *inflow*. The distance between cameras and light sheet was about 600 mm, the focal length of the cameras was 28 mm. No additional seeding was used in order to avoid contamination of the water; the natural load of micro bubbles in the tunnel water turned out to be sufficient anyway. To avoid cavitation (laser reflections on cavitation bubbles can cause damage to the CCD chip), pressure was increased by 0.8 atmospheres. The calibration had to be accomplished in pressurised condition as the observation windows camber a few millimeters, which causes significant distortion in the reconstruction of the velocity fields.

Essential for both experiments is the blackened hub and propeller: Not only will strong reflections destroy pixels in the CCD camera, but – even more important – they

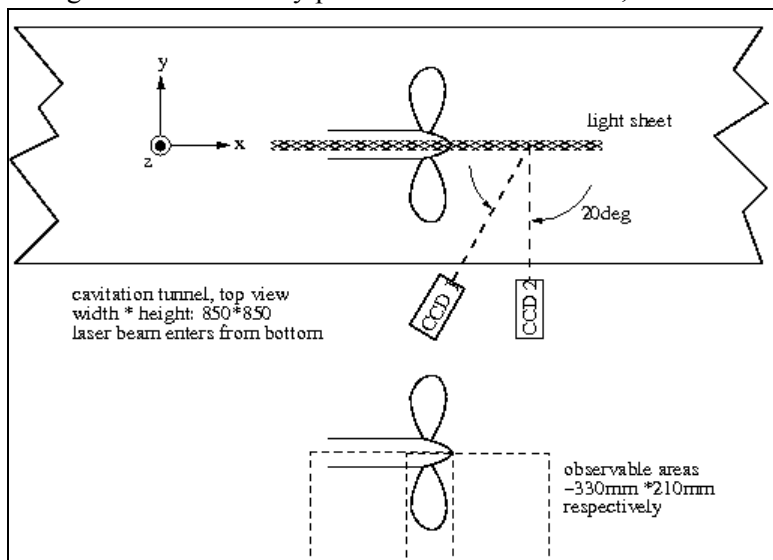


Fig. 5 Schematic sketch of experimental setup in cavitation tunnel (not in scale).

will mess up the measurement, as particles completely outside the actual lightsheet can be illuminated. At best, cross correlation will only create lots of spurious vectors, but in the worst case the analysis will produce velocity fields hardly identifiable as being wrong.

### 3. Image Processing

Data acquisition and analysis is done with the provided software (INSIGHT 3G). The 2D analysis of the left and right particle image displacements is carried out with a multiple pass algorithm with interrogation window deformation, taking into account the resulting vector field of the previous pass. This is especially suitable for flows with high velocity gradients where the particle image displacement may vary across the window. The window size was  $32 \times 32 \text{ px}^2$ . After each pass a mean filter was applied to remove spurious vectors. Finally, another mean filter was utilized to fill holes in the vector field with interpolated data from neighbouring vectors. Fig. 6 shows an example of raw 2D vectors after the very first processing step (left). Several spurious vectors can be detected, especially along the radius of the tip vortex location. As this is the area of high shear flow, several holes are present in the picture. Fig. 6 (right) shows the smoothed and filled vector field after completed processing; the tip vortex and the characteristic acceleration of the tangential velocities caused by the trailing edge vortices can be clearly identified.

Due to the highly turbulent and unsteady nature of the propeller wake this instantaneous velocity field varies between consecutive revolutions. To get a representative velocity distribution for *one* rotational offset a set of shots of this angular position is averaged.

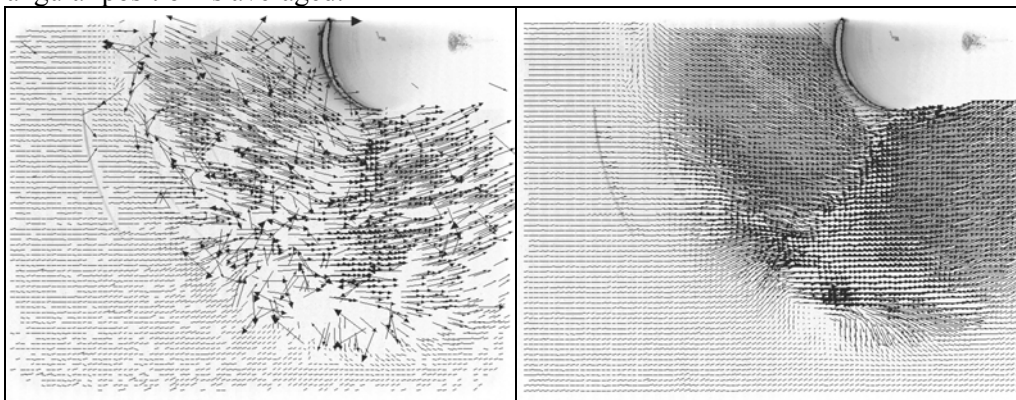


Fig. 6 *Left*: Raw vectors after first evaluation step. *Right*: Validated vector field after full analysis and validation. The crescent-shaped area at the top is the reflection of the laser light sheet on the hub.

### 4. Results

A selected example of the results of the open water tests is shown in Fig. 7. Vectors (top) show the transversal velocity components, and the contours show the axial velocity component, all at  $x/D=0.2$ . The advance ratio was  $J=0.3$ . The tip vortex

is very well distinguishable, and at the upper left corner ( $0^\circ$ ) the beginning of another tip vortex becomes apparent. Fig. 8 shows the smoothed velocity distribution along the marked radii for the normalized axial ( $v_x$ ), tangential ( $v_t$ ) and radial ( $v_r$ ) velocity components.  $v_x/V_a$  clearly shows the segregation between the inner (smaller radii) and outer (larger radii) parts of the tip vortex at  $0.85 \cdot R$ , which in a way marks the centerline of the vortex.

the centerline of the vortex.

Vorticity is defined by the partial derivative of the velocity components:

$$\Omega = \frac{\partial V_y}{\partial x} - \frac{\partial V_x}{\partial y}$$

and its distribution can be seen in Fig. 7 (bottom). The effects induced by the tip vortex and the velocity defect following the trailing edge of the blade can be easily identified; even the shape of the blade becomes visible from the edge vortices (lower right).

Fig. 8 also shows the smoothed vorticity distribution along the specified radii. The slightly curved shape of the maximum's ridge in Fig. 7 can be found

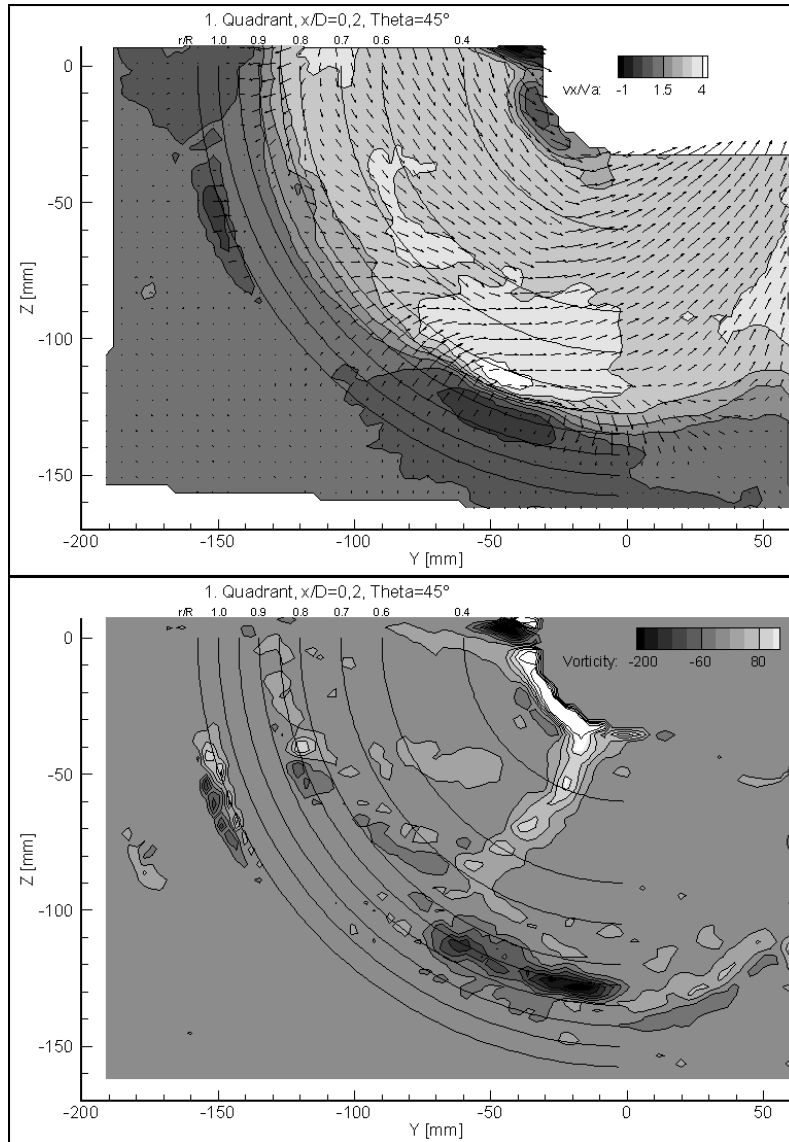


Fig. 7 Top: Resulting axial velocity field from open water test.  $J=0.3$ ,  $x/D=0.2$ , rotational offset  $\Theta=45^\circ$ ,  $n=10 \text{ s}^{-1}$ . Bottom: Vorticity distribution.

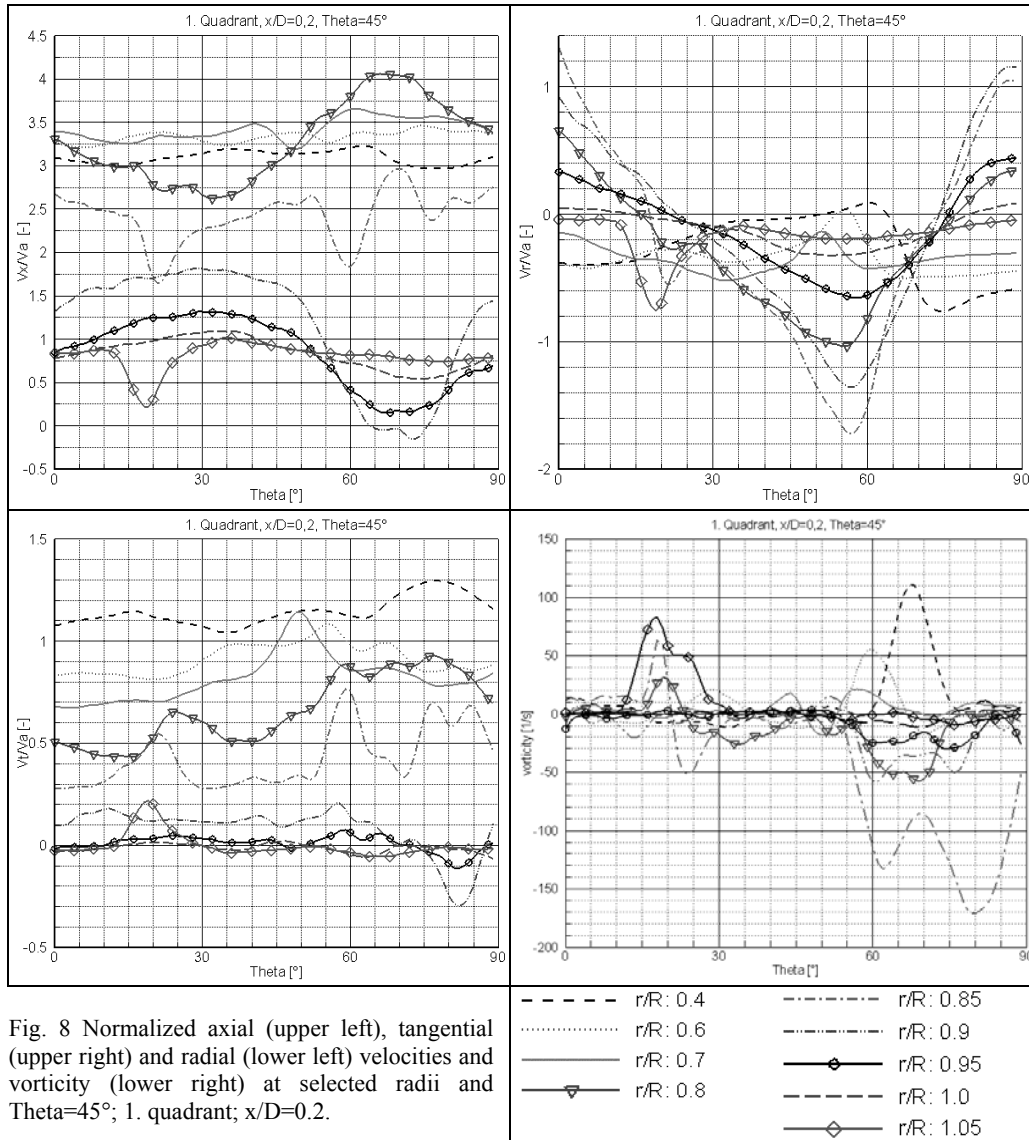


Fig. 8 Normalized axial (upper left), tangential (upper right) and radial (lower left) velocities and vorticity (lower right) at selected radii and Theta=45°; 1. quadrant; x/D=0.2.

again in the distribution of the peaks between 60° and 80°. As pictures were taken via the tilted mirrors, the rotational offset *increases* from 9 o'clock to 6 o'clock position, though the propeller is actually right-handed.

In Fig. 9 an example of the vorticity distribution in the cavitation tunnel experiment is displayed for an advance coefficient of  $J=0.7$ . The strong gradients in the tip vortex and, directionally inverted, in the hub vortex can be seen clearly. Moreover the directionally inverted remainings of the trailing edge vortices can be

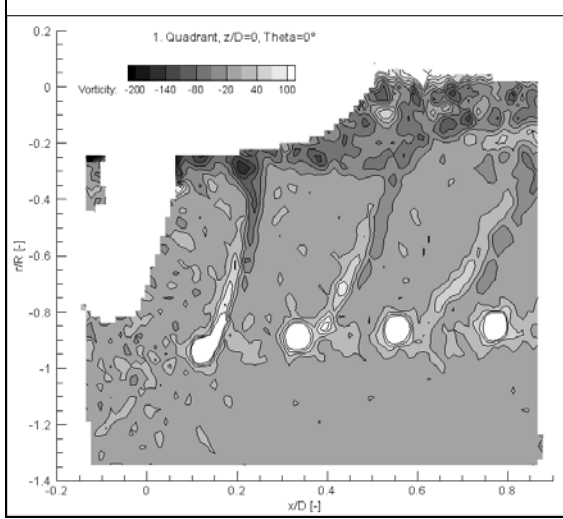


Fig. 9 Vorticity distribution in the cavitation tunnel.  $J=0.7$ .

turbulence intensity, vorticity, strain rate), this technique can well be used for validation of CFD (Computational Fluid Dynamics) calculations, both stationary and unsteady. However, a very fine spatial resolution is required in order to keep up with the detailed results of the measurements. As the investigated volume is large compared to the scale of the vortical structures of interest, the number of grid elements can quickly exceed several million cells, which poses high requirements on the computer hardware. Both experiments were investigated numerically using CFD to solve the RANS equations [5]. A block structured, multi domain grid was developed with about  $2 \cdot 10^6$  control volumes. To close the set of Reynolds Averaged Navier Stokes Equations the SST approach was used and additionally a curvature correction method was applied. The curvature correction adjusts the turbulent production depending on the curvature of the streamlines. Unfortunately, the open water test simulation failed to render the details of the helicoidal tip vortex structure further downstream than about  $0.05D$ . At  $x/D=0.2$  hardly any traces of the tip vortices are to be found in the velocity distribution. One reason could be the combination of turbulence model and grid spacing, as turbulence models in general dissipate turbulent kinetic energy. Following Rung [6], the SST model constant

$$C_{\varepsilon 1} = 1 + 0.44 \cdot \max(1, 0.3S),$$

$S = \left( \frac{k}{\varepsilon} \right) \sqrt{2S_{ij}S_{ij}}$  being the shear rate tensor, can result in a negative production term

for the turbulent viscosity for  $C_{\varepsilon 1} > 2$ :

$$P_{vt} \sim \nu_t \left( \frac{k}{\varepsilon} \right) S_{ii}^2 \left[ \left( \frac{\varepsilon}{P} \right) (C_{\varepsilon 2} - 2) + (2 - C_{\varepsilon 1}) \right]$$

identified above the vorticity cores. Finally, a series of images showing the angular resolved propeller slipstream is presented in Fig. 10. Each of the images results from averaging 10-40 single captures. By averaging these 9 vector fields a mean velocity distribution for the propeller wake can be retrieved, similar to what one gets for example from LDV measurements.

## 5. PIV and CFD

Since the analysis of the SPIV measurement provides most of the interesting variables of the flow (3 velocity components,

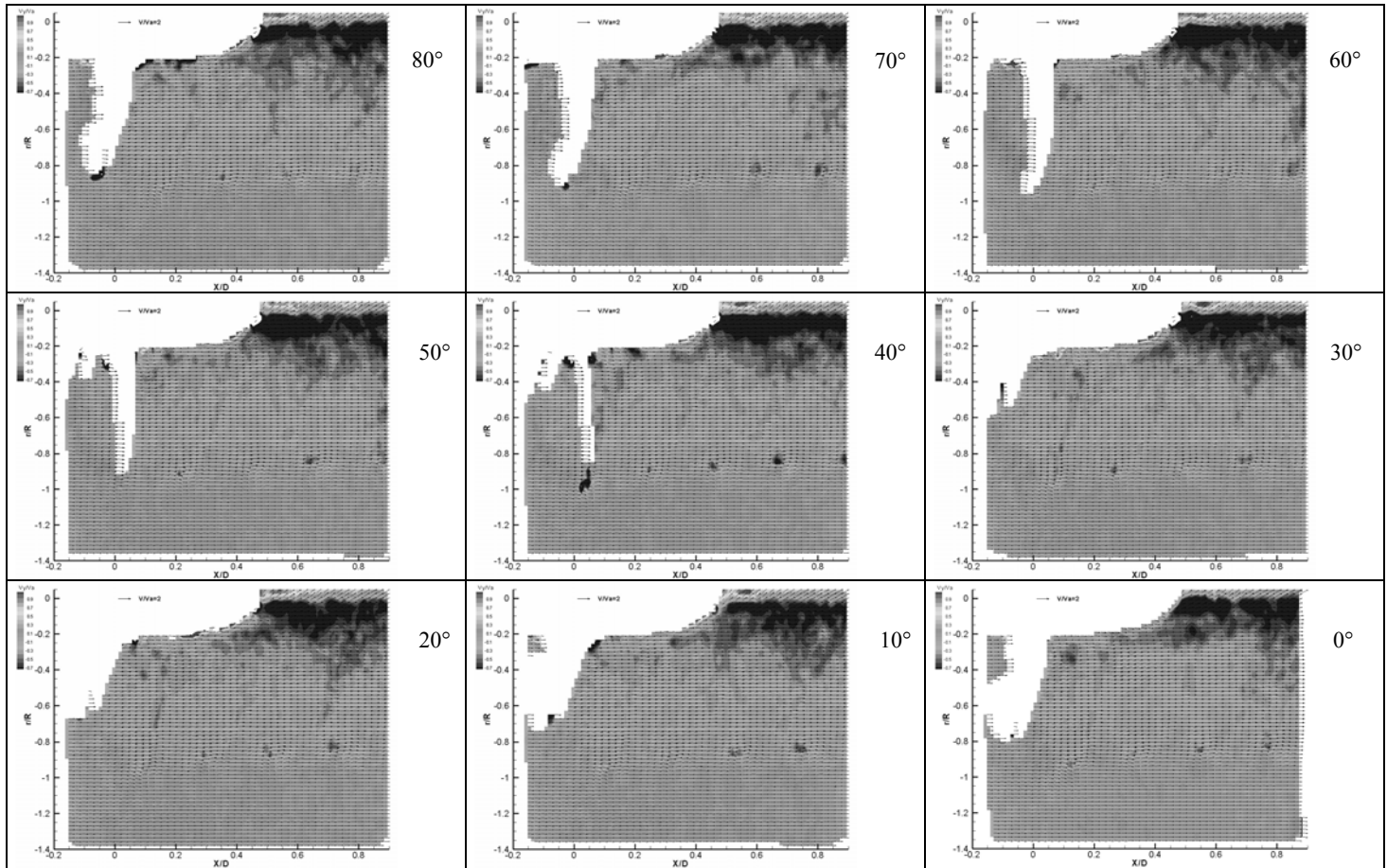


Fig. 10 Angular resolved propeller wake; every picture is phase-averaged from 10-40 pictures. 1. quadrant (positive inflow and rotation);  $J=0.7$ .

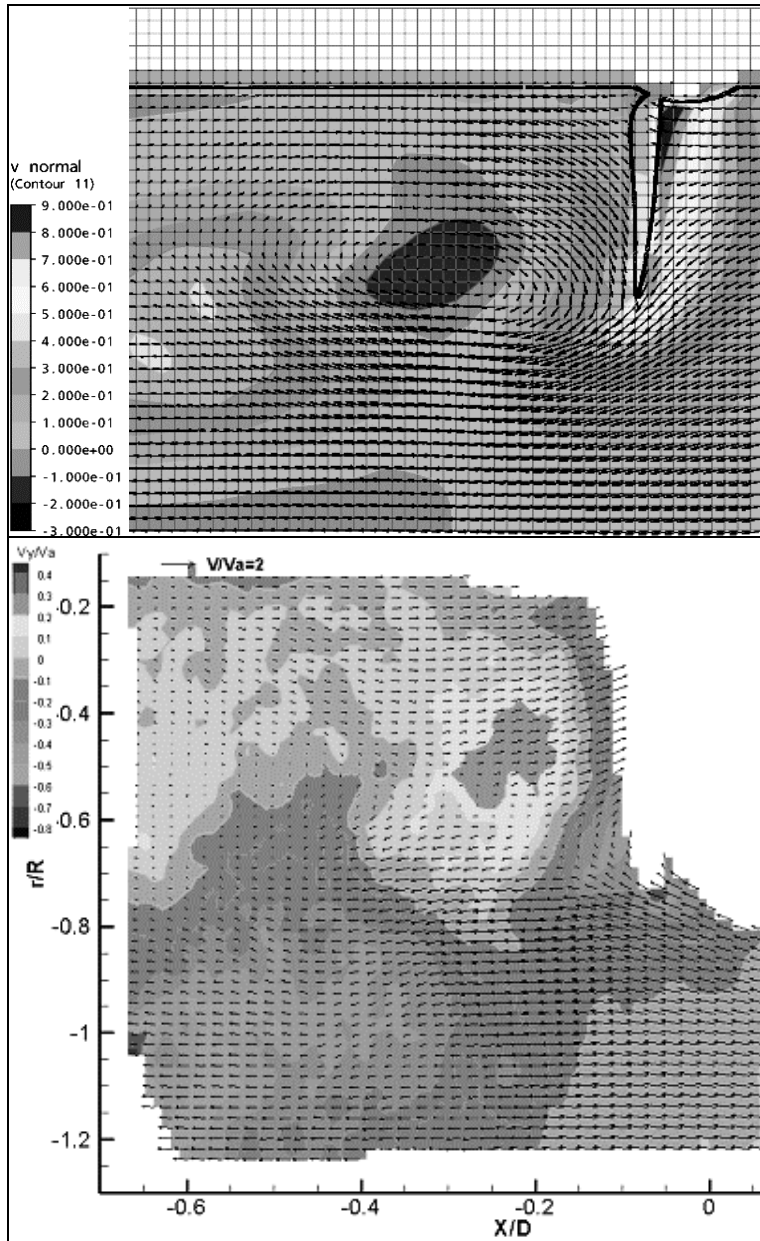


Fig. 11 Velocity field around a propeller in a turbine state, 4. quadrant (negative inflow, positive rotation) in the cavitation tunnel. *Top*: CFD calculation, *Bottom*: PIV measurements. Mind the different scales.

This can rapidly lead to a total decay of turbulence in areas of high shear rates.

The simulation of the cavitation tunnel experiment was more promising. Fig. 11 shows an example of the calculated flow field for the 4. quadrant (negative inflow from right, positive rotation, turbine state) in the cavitation tunnel experiment.

The separating vortices are quite similar, though the simulation places them further downstream. The expansion of the slipstream is slightly stronger in the measurement than in the calculation.

## 6. Conclusions and Outlook

A newly installed submersible stereoscopic Particle Image Velocimetry system at Potsdam Model Basin was introduced. The system can provide detailed insight into flow phenomena which are of vital interest for successful ship and propulsion design and optimisation. Selected results were presented for both the experiments in the towing tank and in the cavitation tunnel. While the measurements revealed vortical structures in great detail in the propeller wake, the CFD calculations did only partly reproduce these structures in the flow. Further investigations have to be done to be able to simulate the flow closer to the conditions measured in the experiment.

In the near future the system will be utilized to measure the wake field behind a model ship with full appendages in various propulsion, inflow and rudder conditions. The measurements will be done in many planes behind the propeller on both sides of the rudder and will hopefully show the flow separation at the inclined rudder. In another experiment the wake behind a wing will be measured in the stationary frame of reference. This requires an extensive conversion of the system, because a very large field of view is requested in a greater operating depth.

### Acknowledgement

This research project was funded by the German Ministry Of Education And Research, BMBF.

### References

- [1] Mach, K.-P.: *Experimentelle Geschwindigkeitsuntersuchungen mittels PIV und LDA in 4 Quadranten für den Modellpropeller VP1455*, Bericht Nr. 3326, Schiffbau-Versuchsanstalt Potsdam, April 2007.
- [2] Courtesy TSI, from personal communication.
- [3] Lee S. J., Paik B. G., Yoon J. H., Lee C.M.: *Three-component velocity field measurements of propeller wake using a stereoscopic PIV technique*, in: *Experiments in Fluids*, vol. 36 (2004) pp. 575–585.
- [4] van Doorne C. W. H., Westerweel J., Nieuwstadt F. T. M.: *Measurement Uncertainty of Stereoscopic-PIV for Flow with Large Out-of-Plane Motion*, in: *Particle Image Velocimetry: Recent Improvements*, Proceedings of EUROPIV 2, 2003, Springer, Berlin, 2004 .
- [5] Rieck, K.: *Berechnung der viskosen Umströmung eines Propellers in 4 Quadranten*, P1423/VP1455, Bericht Nr. 3313, Schiffbau-Versuchsanstalt Potsdam, Januar 2007.
- [6] Rung, Th.: *Statistische Turbulenzmodellierung*, Lecture Notes, [http://www.cfd3.cfd.tu-berlin.de/Lehre/TURB/script/script\\_vollstaendig.pdf](http://www.cfd3.cfd.tu-berlin.de/Lehre/TURB/script/script_vollstaendig.pdf), 2003.